IEEE Access
Multidisciplinary ⋮ Rapid Review ⋮ Open Access Journal

Received 15 June 2024, accepted 28 June 2024, date of publication 10 July 2024, date of current version 24 July 2024.

Digital Object Identifier 10.1109/ACCESS.2024.3425429

RESEARCH ARTICLE

Incorporation of Robust Sliding Mode Control and Adaptive Multi-Layer Neural Network-Based Observer for Unmanned Aerial Vehicles

ZAINAB AKHTAR[1], SYED ABBAS ZILQURNAIN NAQVI[1], MIRZA TARIQ HAMAYUN[2], MUHAMMAD AHSAN[1], AHSAN NADEEM[3], (Member, IEEE), S. M. MUYEEN[4], (Fellow, IEEE), AND ARMAN OSHNOEI[3], (Senior Member, IEEE)

[1]Mechatronics and Control Engineering Department, University of Engineering and Technology, Lahore 54000, Pakistan
[2]Department of Electrical and Computer Engineering, COMSATS University Islamabad (CUI), Lahore Campus, Lahore 54000, Pakistan
[3]Department of Energy, Aalborg University, 9220 Aalborg, Denmark
[4]Department of Electrical Engineering, Qatar University, Doha, Qatar

Corresponding author: S. M. Muyeen (sm.muyeen@qu.edu.qa)

Open Access funding provided by the Qatar National Library.

ABSTRACT The control and state estimation of Unmanned Aerial Vehicles (UAVs) provide significant challenges due to their complex and nonlinear dynamics, as well as uncertainties arising from factors such as sensor noise, wind gusts, and parameter fluctuations. Neural network-based methods tackle these problems by accurately approximating unknown nonlinearities through training on input-output data. This paper proposes an adaptive Multi-layer Neural Network (MLNN) Luenberger observer-based control for altitude and attitude tracking of a quadrotor UAV. The MLNN observer, employing a modified back-propagation algorithm, is used for the quadrotor's state estimation. The adaptive nature of the proposed observer helps mitigate the effects of parameters such as wind gusts, measurement noise, and parameter variations. Subsequently, a sliding mode controller is designed based on the observed states to track the reference trajectories. Lyapunov stability is ensured by using the modified back-propagation weight update rule for the proposed MLNN observer. Simulation results demonstrate superior tracking performance of the proposed observer compared to the Sliding Mode Observer (SMO) and a Single Hidden Layer Neural Network (SHLNN) observer, even in the presence of the aforementioned parameters.

INDEX TERMS Back-propagation algorithm, multiple hidden layers perceptron (MLP), neural network (NN) observer, sliding mode controller (SMC), sliding mode observer, UAVs.

I. INTRODUCTION

In recent years, unmanned air vehicles (UAVs) have gained popularity in various fields such as military, civil, industrial, and agricultural applications. These include environmental protection, reliable navigation, exploration of hostile areas that are dangerous for humans to enter, and many other domestic applications [1], [2]. Autonomous navigation has been made possible due to recent technological advancements in mini drones at a reasonable cost [3]. The control of UAVs is a more challenging task as they experience undesirable forces such as external aerodynamic effects i.e., wind gusts and sensor noise can lead to instability or crash of the vehicles. Therefore, these problems are essential and should be considered for safe navigation.

Accurate information on all plant model states is necessary for improved control and navigation. In control system theory, controller design depends on state information derived from the system's output. While suitable sensors can be used to acquire this information, their high cost, limited availability, and accuracy difficulties make this impractical in some circumstances. The alternative is to use state observers

The associate editor coordinating the review of this manuscript and approving it for publication was Guillermo Valencia-Palomo.

to estimate the system's states. An effective state observer minimizes errors between the actual and estimated states of the system. Thus, there is a need for such observers that can estimate the states of a UAV quadrotor in the presence of wind gusts, sensor noise, and parameter variations. Several conventional observers have been studied in recent years for state estimation. In [4], a disturbance-based H-infinity controller is proposed for a vertical takeoff and landing UAV, and its performance is tested under different disturbance effects. A fuzzy state observer has been proposed for a multiple-input-multiple-output system (MIMO) [5]. The main objective is to design an observer-based fuzzy feedback controller for a MIMO helicopter model with unknown input delays and control gain. A similar study [6] suggests a fuzzy observer feedback control of a MIMO system. However, designing, and tuning fuzzy sets and rules can be time-consuming, given that fuzzy observers heavily rely on data and expert knowledge to define these sets and rules. Optimal Kalman filters [7], Extended Kalman filter (EKF) [8], and Unscented Kalman filters (UKF) [9] have been used in the literature for state estimation purposes in UAVs. However, as they rely on the system's dynamics, the nonlinearities in the system's dynamics affect their estimation performance, leading to stability and convergence issues. Sliding mode observer has been applied in state estimation due to its robustness and disturbance rejection properties [10], [11], [12], [13]. SMO for fault estimation has been discussed in [14] and [15]. Although, sliding mode-based observers are robust to external disturbances, they are sensitive to sensor noise and parameter variations. Adaptive high-gain observers are presented in [16] and [17]; however, they also have drawbacks. First, they require complete knowledge of the system's dynamics, and second, they are highly sensitive to noise. Another high-gain observer for robots with elastic joints is discussed in [18], but it requires the system model information, which is not always available. Conventional observers face limitations in learning complex nonlinear functions and uncertainties. They require a perfect model of the system, which is not always available, and cannot completely reject the effects of measurement noise and parameter variations. To address such issues, neural network-based techniques have been recently integrated with conventional observers.

The neural network-based observer schemes have been used in various applications because of their capability to learn the highly nonlinear dynamics of plant models, which are difficult to learn by conventional state estimators. Specifically, they have gained importance in UAV applications [19], [20], which require highly reliable control and state estimation schemes. They can handle unknown uncertainties in nonlinear systems. Robust control techniques based on fuzzy logic and neural networks have been developed for uncertain systems [6], [21]. In [22] an adaptive neural network observer-based fuzzy model predictive controller is proposed for a hypersonic vehicle (HV). The paper proposes a neural network disturbance observer-based fuzzy controller for an HV, which considers uncertainties in aerodynamic coefficients and external disturbances. However, the observer scheme does not consider or estimate the effects of noise and parameter variations, which are significant aspects studied in this paper. Secondly, the drawback of fuzzy rules is the complex process of designing and tuning them for optimal performance. In [23], a Radial Basic Function Neural Network (RBFNN) based disturbance observer technique is proposed to estimate unknown disturbances and model uncertainties for the tracking control of multiple UAVs. In [24], an RBFNN-based disturbance observer is proposed for the attitude and altitude control of a UAV in the presence of disturbances and model uncertainties. In both studies, the efficiency of the disturbance observers was tested under model uncertainty and various levels of environmental disturbances. Although disturbance observers are well-known for estimating disturbances, they are not typically used for noise estimation [25] as their designs and operational principles are not suited for the high frequency and random nature of noise. For enhancing the Kalman filter attitude estimation capability, a neuro-fuzzy network was proposed in [26]. In [27], a sensor fault detection scheme is proposed using an adaptive neural network-based observer in which the weights are updated using an extended Kalman filter for a quadrotor UAV in the presence of noise and disturbances. In a similar work [28], an extended Kalman filter updates the weighting parameters of a neural network-based observer for a nonlinear aircraft model. However, using Kalman filter weight updates in neural networks can have certain drawbacks as compared to traditional Artificial Neural Network (ANN) weight updates. Kalman filters can be sensitive to outliers and noisy data, impacting the accuracy of weight updates, unlike ANNs, which are more robust. Secondly, Kalman filters are computationally intensive and complex to implement, making them harder to manage than ANN weight update algorithms.

Several ANN schemes have been studied in recent literature due to their robustness and effectiveness in learning nonlinearities. A neural network-based sliding mode observer for a quadcopter is proposed in [29] to overcome the effects of bounded disturbances. A neural network-based intelligent attitude estimation sensor has been suggested for the GPS navigation model [30]. In [31], a single hidden layer (SHL) neural network-based observer is proposed for the state estimation of a quadrotor UAV which is insensitive to measurement noise. The observer uses a single hidden layer neural network with a sigmoid activation function to estimate a non-linear function in the quadrotor system. To compensate for the effects of model uncertainties and disturbances, the authors in [32] proposed a guidance and control technique based on a neural network observer for a missile. In [33], a multi-layer neural network-based observer estimates the states of an induction motor. The technique estimates the unknown uncertainty term in the model of

the induction motor but does not consider the effects of sensor noise. In [34], a disturbance observer is integrated with a multi-layer exponential sliding mode controller to accommodate the effects of disturbances and parameter uncertainties in a UAV. In the study [35], a deep learning-based Kalman filter for state estimation is proposed for multi-rotor which is validated in the presence of noise only. In [36], a single-layer neural network-based observer for a UAV using a back-propagation weight update law is used to eliminate disturbances effects. In [37], a back-propagation-based disturbance rejection scheme has been proposed for the attitude control of a quadrotor. The study considered only one varying parameter, i.e., mass variation during their simulation results. In the mentioned works [29], [30], [31], [32], [33], [34], [35], [36], [37], quadrotor control and state estimation have been carried out without simultaneously considering wind disturbances, noise, and parameter variations, which poses significant challenges in practical applications. Furthermore, the stability analysis in the earlier mentioned works is confined to a single layer, while we have extended it to a multi-layer back-propagation algorithm.

To overcome the above mentioned limitations, this study introduces a multi-layer neural network Luenberger observer-based controller design for a quadrotor UAV. The state information estimated by the MLNN observer is given to SMC to track the reference altitude and attitude trajectories. The adaptive weights help to eliminate the effects of measurement noise, wind gusts, and parameter variations. The adoption of the multi-layer scheme is motivated by the fact that multi-layer architecture requires a lesser number of trainable parameters (neurons) than the single-layer implementation for achieving similar performance and accuracy. Secondly, if the number of hidden layers becomes large, MLP significantly outperforms single-layer neural networks on data sets of very large size. The Lyapunov stability proof of the proposed MLNN observer is also provided which is an extension of the Lyapunov proof for a single-layer NN proposed in [33]. A comparison of the proposed observer is made with a single hidden layer neural network observer proposed in [36] and a sliding mode observer [14] for the quadrotor's state estimation.

To the best of the author's knowledge, the main contributions of the proposed approach are as follows:

- Design of a multi-layer neural network-based Luenberger observer with adaptive weights and bias terms using a modified back-propagation algorithm with gradient scaling.
- Comparison of the performance of the proposed MLNN Luenberger observer with the Sliding Mode and SHLNN observer in the presence of parameter variations, external disturbance, and sensor noise.
- Unlike the previous works [29], [30], [31], [32], [33], [34], [35], [36], [37], the Lyapunov stability analysis is extended to a multi-layer modified back-propagation algorithm with gradient scaling, which according to the author's best knowledge is not available in the literature.

The rest of this paper is organized into five sections. Section II presents the nonlinear mathematical model of the quadrotor UAV. The problem statement and the proposed observer-based control technique's formulation are discussed in Section III, while Section IV features the simulation results of the nonlinear observers. Finally, the concluding remarks and future work are discussed in Section V.

II. NONLINEAR MATHEMATICAL MODEL OF QUADROTOR

The quadrotor has six degrees of freedom with only four propellers, making it an under-actuated system. The assumptions considered for the quadrotor model presented in the paper are as follows [3]:

- The quadrotor has a rigid and symmetric structure, Next point plant's center of gravity is at the origin of the body's fixed frame,
- The rotors are rigid,
- The drag force, and upward thrust are proportional to the square of the speeds of the rotors.
- The inertial matrix used is diagonal.

The rotations about the x, y, and z-axis are roll(ϕ), pitch(θ), and yaw(ψ) respectively, while p, q, and r denote the angular velocity in the body frame. $\Omega(i = 1, 2, 3, 4)$ represents the i^{th} rotor speed. A quadrotor UAV has twelve states, namely, x, y, and z positions, and their rates $\dot{x}$, $\dot{y}$ and $\dot{z}$ from the earth's frame of reference respectively. The remaining six include the roll, pitch, and yaw angles denoted by ϕ, θ and ψ respectively along with their angular velocities $\dot{\phi}$, $\dot{\theta}$ and $\dot{\psi}$. The nonlinear dynamical equations of the quadrotor are as follows [3]:

$$\begin{cases} \ddot{x} = (cos\phi sin\theta cos\psi + sin\phi sin\psi)\dfrac{U_1}{m} \\ \ddot{y} = (cos\phi sin\theta sin\psi - sin\phi cos\psi)\dfrac{U_1}{m} \\ \ddot{z} = -g + (cos\phi cos\theta)\dfrac{U_1}{m} \\ \ddot{\phi} = \dot{\theta}\dot{\psi}\left(\dfrac{I_y - I_z}{I_x}\right) - \dfrac{I_r}{I_x}\dot{\theta}\Omega + \dfrac{U_2}{I_x} \\ \ddot{\theta} = \dot{\phi}\dot{\psi}\left(\dfrac{I_z - I_x}{I_y}\right) - \dfrac{I_r}{I_y}\dot{\phi}\Omega + \dfrac{U_3}{I_y} \\ \ddot{\psi} = \dot{\phi}\dot{\theta}\left(\dfrac{I_x - I_y}{I_z}\right) + \dfrac{U_4}{I_z} \end{cases} \tag{1}$$

where U_1, U_2, U_3 and U_4 are the control inputs defined later in (36). The parameters of the quadrotor are given in Table 1, taken from [3], and the layout is shown in Figure 1. The quadrotor UAV has the following states:

$$[x\ \dot{x}\ y\ \dot{y}\ z\ \dot{z}\ \phi\ \dot{\phi}\ \theta\ \dot{\theta}\ \psi\ \dot{\psi}] = [x_1\ x_2\ x_3\ x_4\ x_5\ x_6\ x_7\ x_8\ x_9\ x_{10}\ x_{11}\ x_{12}] \tag{2}$$

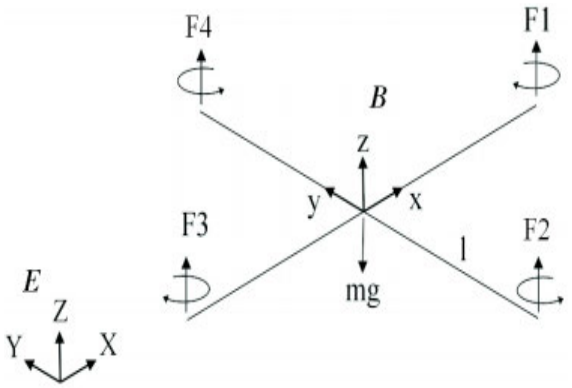

FIGURE 1. Structure of a quadrotor UAV.

TABLE 1. Parameters of the quadrotor.

Parameters	Values	Explanation
$Ix(kg.m^2)$	$7.5\text{x}10^{-3}$	Inertia of X-axis
$Iy(kg.m^2)$	$7.5\text{x}10^{-3}$	Inertia of Y-axis
$Iz(kg.m^2)$	$1.3\text{x}10^{-2}$	Inertia of Z-axis
$Ir(kg.m^2)$	$6\text{x}10^{-5}$	Inertia of Rotor
$b(N.s^2)$	$3.13\text{x}10^{-5}$	Coefficient of Thrust
$d(m.s^2)$	$7.15\text{x}10^{-7}$	Drag Coefficient
$m(kg)$	0.65	mass
$l(m)$	0.26	Arm length

The state-space form representation of the dynamical model of UAV presented in (2) is as follows:

$$\begin{cases} \dot{x}_1 = \dot{x} = x_2 \\ \dot{x}_2 = \ddot{x} = (cosx_7 sinx_9 cosx_{11} + sinx_7 sinx_{11})\dfrac{U_1}{m} \\ \dot{x}_3 = \dot{y} = x_4 \\ \dot{x}_4 = \ddot{y} = (cosx_7 sinx_9 sinx_{11} - sinx_7 cosx_{11})\dfrac{U_1}{m} \\ \dot{x}_5 = \dot{z} = x_6 \\ \dot{x}_6 = \ddot{z} = -g + (cosx_7 cosx_9)\dfrac{U_1}{m} \\ \dot{x}_7 = \dot{\phi} = x_8 \\ \dot{x}_8 = \ddot{\phi} = x_{10}x_{11}\left(\dfrac{I_y - I_z}{I_x}\right) - \dfrac{I_r}{I_x}x_{10}\Omega + \dfrac{U_2}{I_x} \\ \dot{x}_9 = \dot{\theta} = x_{10} \\ \dot{x}_{10} = \ddot{\theta} = x_8 x_{12}\left(\dfrac{I_z - I_x}{I_y}\right) - \dfrac{I_r}{I_y}x_8\Omega + \dfrac{U_3}{I_y} \\ \dot{x}_{11} = \dot{\psi} = x_{12} \\ \dot{x}_{12} = \ddot{\psi} = x_8 x_{10}\left(\dfrac{I_x - I_y}{I_z}\right) + \dfrac{U_4}{I_z} \end{cases} \tag{3}$$

III. PROBLEM STATEMENT

The nonlinear dynamics of quadrotor system described in (1) can be written into a general form:

$$\begin{aligned} \dot{x}_M(t) &= A_M x_M(t) + g(x_M, u_M) \\ y_M(t) &= C_M x_M(t) \end{aligned} \tag{4}$$

where $x_M(t) \in \mathbb{R}^m$, $u_M(t) \in \mathbb{R}^n$, and $y_M(t) \in \mathbb{R}^r$ are the states, input, and output vectors respectively. while A_M, B_M, and C_M represent the system, input, and output matrices, respectively, and $g(x_M, u_M)$ is an unknown function to be estimated by the MLNN observer. We have considered a MLNN architecture having L layers, where z_0 is the input layer, $z_{1,\ldots L-1}$ are hidden layers, and z_L is the output layer. According to [36], any non-linear function can be written as a combination of activation and ideal weight functions in the following manner:

$$g(x_M, u_M) = z_L + \epsilon(x) \tag{5}$$

where z_L represents the output layer of a multi-layer neural network which can be written in terms of sigmoid activation function [38] as:

$$z_L = \sigma\left(w_L z_{L-1} + b_L\right)$$

where w_L, b_L represents the weights and bias terms of the L^{th} layer of the MLNN architecture, and $\sigma(.)$ denotes the sigmoid activation function applied in the hidden layers. z_L can be further defined as:

$$z_L = w_L z_{L-1}$$

where,

$$z_{L-1} = \sigma^0(w_{L-1}, \ldots w_1, b_{L-1}, \ldots b_1, z_0),\ z_0 = [x_M, u_M] \tag{6}$$

In (6), w_i and b_i represent the weights and bias terms of the i^{th} layer. By using (6), the equation (5) can be expressed as:

$$g(x_M, u_M) = w_L \sigma^0(w_{L-1}, \ldots w_1, b_{L-1}, \ldots b_1, z_0) + b_L + \epsilon(x) \tag{7}$$

where z_0 is the input layer and $\epsilon(x)$ denotes the approximation error of the neural network, ensuring $\|\epsilon(x))\| \leq \epsilon_N$, where ϵ_N is a positive number.

We identified two main problems in this study. The first is state estimation in the presence of measurement noise, disturbances, and parameter variations. The second is control based on the estimated states. The upcoming section focuses on the observer design, followed by a description of the sliding mode control design.

Remarks: In this work, we considered the following states available at the output

$$[x\ y\ z\ \phi\ \theta\ \psi] = [x_1\ x_3\ x_5\ x_7\ x_9\ x_{11}\ ] \tag{8}$$

In this section, we considered a general state-space form (4) to formulate a MLNN-based Luenberger observer. The state vector for quadrotor attitude dynamics is

$$[\phi, \theta, \psi, p, q, r]^T = [\,x_7\ x_8\ x_9\ x_{10}\ x_{11}\ x_{12}\,] \tag{9}$$

A. PROPOSED MLNN OBSERVER DESIGN

The proposed observer design utilizing the multi-layer neural network for the system (4) is as follows [36]:

$$\begin{aligned}\dot{\hat{x}}_M(t) &= A_M\hat{x}_p(t) + \hat{g}(\hat{x}_M, u_M) + F_M\left(y_M(t) - \hat{y}_M(t)\right)\\ \hat{y}_M(t) &= C_M\hat{x}_M(t)\\ \hat{g}(\hat{x}_M, u_M) &= \hat{w}_L\sigma^0\left(\hat{w}_{L-1}, \cdots \hat{w}_1, \hat{b}_{L-1}, \cdots, \hat{b}_1, \hat{z}_0\right) + \hat{b}_L\end{aligned} \tag{10}$$

here $\hat{x}_M(t)$, $\hat{y}_M(t)$, and $F_M \in \mathbb{R}^{r\times m}$ represent the estimated states, outputs, and observer gains respectively, while $\hat{g}(\hat{x}_M, u_M)$ is the unknown function estimated by the multi-layer neural network observer. $\hat{w}_i$ and $\hat{b}_i$ refer to the neural network's weights and bias terms, respectively. The estimation errors for the state and output are:

$$\begin{aligned}e_M(t) &= x_M(t) - \hat{x}_M(t);\\ e_{y_M}(t) &= y_M(t) - \hat{y}_M(t)\end{aligned} \tag{11}$$

The system's error dynamics, following the addition and subtraction of $\left[\hat{w}_L\sigma^0\left(\hat{w}_{L-1}, \cdots \hat{w}_1, \hat{b}_{L-1}, \cdots, \hat{b}_1, \hat{z}_0\right)\right]$ become:

$$\begin{aligned}\dot{e_M}(t) =& G_M e_M(t) + \left[e_{w_L}\sigma^0\left(\hat{w}_{L-1}, \cdots \hat{w}_1, \hat{b}_{L-1}, \cdots \hat{b}_1, \hat{z}_0\right)\right]\\ &+ e_{b_L} + \aleph(t)\\ e_{y_M}(t) =& C_M e_M(t).\end{aligned} \tag{12}$$

here $e_{w_L} = w_L - \hat{w}_L, e_{b_L} = b_L - \hat{b}_L, G_M = A_M - F_M C_M$ and $\aleph(t) = w_L\left[\sigma^0\left(w_{L-1}, \cdots w_1, b_{L-1}, \cdots b_1, z_0\right) - \sigma^0\left(\hat{w}_{L-1}, \cdots \hat{w}_1, \hat{b}_{L-1}, \cdots \hat{b}_1, \hat{z}_0\right)\right] + \epsilon(x)$ is disturbance within bounds ensuring $\|\aleph\| \leq \bar{\aleph}$ where $\bar{\aleph}$ is a positive constant. In this study, we utilize a modified back-propagation algorithm [36] to optimize the weights of the MLNN, aiming to minimize the cost function as follows:

$$J_M = \frac{1}{2}e_{y_M}^T e_{y_M} \tag{13}$$

By applying the chain rule, the partial derivative of (13) for $i = 1, \ldots, L-1$, is obtained as

$$\frac{\partial J_M}{\partial \hat{w}_i} = diag(\frac{\partial J_M}{\partial \hat{z}_i})^T \frac{\partial \hat{z}_i}{\partial \hat{w}_i} \tag{14}$$

where $\frac{\partial J_M}{\partial \hat{z}_i} = \frac{\partial J_M}{\partial e_{y_M}}\frac{\partial e_{y_M}}{\partial e_M}\frac{\partial e_M}{\partial \hat{z}_L}\frac{\partial \hat{z}_L}{\partial \hat{z}_{L-1}}\frac{\partial \hat{z}_{L-1}}{\partial \hat{z}_{L-2}}\cdots\frac{\partial \hat{z}_{i+1}}{\partial \hat{z}_i}$, $\frac{\partial J_M}{\partial e_{y_M}} = e_{y_M}^T$, $\frac{\partial e_{y_M}}{\partial e_M} = C_M$ and $\frac{\partial e_M}{\partial \hat{z}_L} = G_M^{-1}B_M$. As $e_{y_M}(t) = C_M e_M(t)$, substituting the expression of $\frac{\partial J_M}{\partial e_{y_M}}, \frac{\partial e_{y_M}}{\partial e_M}, \frac{\partial e_M}{\partial \hat{z}_L}$ in (14):

$$\frac{\partial J_M}{\partial \hat{w}_i} = diag\left(e_M^T C_M^T C_M G_M^{-1} B_M \frac{\partial \hat{z}_L}{\partial \hat{z}_{L-1}}\frac{\partial \hat{z}_{L-1}}{\partial \hat{z}_{L-2}}\frac{\partial \hat{z}_{i+1}}{\partial \hat{z}_i}\right)^T \frac{\partial \hat{z}_i}{\partial \hat{w}_i} \tag{15}$$

where

$$\begin{aligned}\frac{\partial \hat{z}_L}{\partial \hat{z}_{L-1}} &= \hat{w}_L\\ \frac{\partial \hat{z}_{i+1}}{\partial \hat{z}_i} &= diag\left(\sigma'\left(\hat{w}_{i+1}\hat{z}_i + \hat{b}_{i+1}\right)\right)\hat{w}_{i+1}\\ \frac{\partial \hat{z}_i}{\partial \hat{w}_i} &= \sigma'\left(\hat{w}_i\hat{z}_{i-1} + \hat{b}_i\right)\hat{z}_{i-1}^T\end{aligned}$$

This study introduced a modified back-propagation algorithm proposed in [33] and [36], using the following weight update equations:

$$\begin{aligned}\dot{\hat{w}}_i &= \frac{-\beta_i}{\prod_{j=i+1}^{L-1}\|\hat{w}_j + \xi_M\|}\frac{\partial J_M}{\partial \hat{w}_i} - K_M\|e_M\|\hat{w}_i\\ \dot{\hat{w}}_L &= -\eta_L\frac{\partial J_M}{\partial \hat{w}_L} - K_M\|e_M\|\hat{w}_L\\ \dot{\hat{b}}_i &= \frac{-\gamma_i\|\hat{b}_L\|}{\prod_{j=i+1}^{L}\|\hat{w}_j + \xi_M\|}\frac{\partial J_M}{\partial \hat{b}_i} - K_M\|e_M\|\hat{b}_i\\ \dot{\hat{b}}_L &= -\gamma_L\frac{\partial J_M}{\partial \hat{b}_L} - K_M\|e_M\|\hat{b}_L\end{aligned} \tag{16}$$

where $\beta_{i\cdots L}, \gamma_{i\cdots L}$ denote the learning rates and K_M are positive terms. Consiering $T_{M_L} = -\beta_L C_M^T C_M G_M^{-1} B_M$, $R_{M_L} = -\gamma_L B_M^T G_M^{-1} C_M^T C_M$. By inserting (15) in (16), we obtain:

$$\begin{aligned}\dot{\hat{w}}_i &= \frac{-\beta_i}{\prod_{j=i+1}^{L-1}\|\hat{w}_j + \xi_M\|}diag(\frac{\partial J_M}{\partial \hat{z}_i}^T)\acute{\alpha}(w_i z_{i-1} + b_i)z_{i-1}^T\\ &\quad - K_M\|e_M\|\hat{w}_i\\ \dot{\hat{b}}_i &= \frac{-\gamma_i\|\hat{b}_L\|}{\prod_{j=i+1}^{L}\|\hat{w}_j + \xi_M\|}diag(\frac{\partial J_M}{\partial \hat{z}_i}^T)\acute{\alpha}(w_{L-1} z_{L-2} + b_{L-1})\\ &\quad - K_M\|e_M\|\hat{b}_i\end{aligned} \tag{17}$$

Using ξ_M to avoid singularities, we derive the update law for the output layer as:

$$\dot{\hat{w}}_L = diag(e_M^T T_L)^T z_{L-1}^T - K_M\|e_M\|\hat{w}_L \tag{18}$$

and $\acute{\sigma}(w_i z_{i-1} + b_i)$ is the derivative of $\sigma(w_i z_{i-1} + b_i)$ in (17).

Stability Analysis: For showing asymptotic stability, the "direct theorem of Lyapunov" is very frequently used in the control literature. Lyapunov stability proof of the proposed MLNN-based Luenberger observer is an extension of Lyapunov proof for a single layer NN proposed in [33] and [36] with modification in update equations of modified backpropagation with gradient scaling. The following Lyapunov function is proposed for the multilayer case:

$$g = \frac{1}{2}e_M^T P_M e_M + \sum_{i=1}^{L}\frac{1}{2}tr(e_{w_i}^T e_{w_i}) + + \sum_{i=1}^{L}\frac{1}{2}e_{b_i}^T e_{b_i} \tag{19}$$

where $P_M = P_M^T > 0$ which satisfies,

$$G_M^T P_M + P_M G_M = -Q_M \tag{20}$$

[0] tr denotes the trace operator.

for some positive definite matrix Q_M such that $g > 0\ \forall x_M \neq 0$ and $\dot{g}(0) = 0$. The time-derivative of (19) is obtained as

$$\dot{g} = \frac{1}{2}\dot{e_M}^T P_M e_M + \frac{1}{2} e_M^T P \dot{e}_M + \sum_{i=1}^{L} \frac{1}{2} tr(e_{w_i}^T \dot{e}_{w_i}) + \sum_{i=1}^{L} \frac{1}{2} e_{b_i}^T \dot{e}_{b_i} \tag{21}$$

where e_M is observer error already defined in (12), $\dot{e}_{w_i}$ denotes the derivative of weight error defined as

$$\begin{aligned} \dot{e}_{w_i} &= \frac{\beta_i}{\prod_{j=i+1}^{L-1} \|\hat{w}_j + \xi_M\|} diag(\frac{\partial J_P}{\partial \hat{z}_i}^T) \acute{\sigma}(w_i z_{i-1} + b_i) z_{i-1}^T \\ &\quad - K_M \|e_M\| \hat{w}_i \\ \dot{e}_{w_L} &= -diag(e^T T_{M_L})^T z_{L-1}^T - K_M \|e_M\| \hat{w}_L \end{aligned} \tag{22}$$

and $\dot{e}_{b_i}$ is the derivative of bias error defined as

$$\begin{aligned} \dot{e}_{b_i} &= \frac{\beta_i \|\hat{b}_L\|}{\prod_{j=i+1}^{L} \|\hat{w}_j + \xi_M\|} diag(\frac{\partial J_M}{\partial \hat{z}_i}^T) \acute{\sigma}(w_{L-1} z_{L-2} + b_{L-1}) \\ &\quad - K_M \|e_M\| \hat{b}_i \\ \dot{e}_{b_L} &= -R_{M_L} e_M + K_M \|e_M\| \hat{w}_L \end{aligned} \tag{23}$$

where $\dot{e}_{w_L} = \dot{w}_L - \dot{\hat{w}}_L$ and $\dot{e}_{b_L} = \dot{b}_L - \dot{\hat{b}}_L$. Putting the terms $\sigma'(t)$, $\dot{e}_{w_i}$, $\dot{e}_{b_i}$ and (20) in (21) we get:

$$\begin{aligned} \dot{g} &= \frac{1}{2} e_M^T Q_M e_M + e_M^T P_M [e_{w_L} \sigma^0 (w_{L-1}, \ldots w_1, b_{L-1}, \ldots b_1, z_0) \\ &\quad + \sigma'(t) + e_{b_L}] + \sum_{i=1}^{L-2} tr[e_{w_i}^T \frac{\beta_i}{\prod_{j=i+1}^{L-1} \|\hat{w}_j + \xi_M\|} diag(\frac{\partial J_M}{\partial \hat{z}_i}^T) \\ &\quad \times \acute{\sigma}(w_i z_{i-1} + b_i) z_{i-1}^T - K_M \|e_M\| \hat{w}_i] + tr[e_{w_{L-1}}^T diag(\frac{\partial J_M}{\partial \hat{z}_{L-1}}^T) \\ &\quad \times \acute{\sigma}(w_{L-1} z_{L-2} + b_{L-1}) z_{L-2}^T - K_M \|e_M\| \hat{w}_{L-1}] + tr[-e_M^T{}_{w_L} \\ &\quad \times diag(e_M^T T_L)^T z_{L-1}^T + K_M \|e_M\| \hat{w}_L] + \sum_{i=1}^{L-2} e_{b_i}^T \\ &\quad \times [\frac{\gamma_i \|\hat{b}_L\|}{\prod_{j=i+1}^{L} \|\hat{w}_j + \xi_M\|} diag(\frac{\partial J_M}{\partial \hat{z}_i}^T) \acute{\sigma}(w_{L-1} z_{L-2} + b_{L-1}) \\ &\quad - K_M \|e_M\| \hat{b}_i] + e_{b_L}^T [-R_L e_M + K_M \|e_M\| \hat{b}_L] \end{aligned} \tag{24}$$

By assuming that $\|\sigma'\| \leq \sigma_0^M$, $\|b_i\| \leq \|b_{M_i}\|$ and $\|w_i\| \leq w_{M_i}$ for all $i = 1 \cdots L-1$,the subsequent inequality is as follows:

$$\begin{aligned} \dot{g} &\leq -\frac{1}{2} \eta_{min} Q_M \|e_M\|^2 + \|e_M\| \|P_M\| (\|e_{M\,w_L}\| \sigma_M^0 + \sigma') \\ &\quad + \|e_M\| \|P_M\| \|e_{b_L}\| + \sum_{i=1}^{L-1} \|e_M\| \|e_{w_i}\| 2K_{M_i} \|\hat{w}_L\| \\ &\quad + K_M \|e_M\| \sum_{i=1}^{L-1} \left(w_{M_i} \|e_{w_i}\| - \|e_{w_i}\|^2 \right) \\ &\quad + |e_M\| \|T_{M_L}\| \|e_{w_L}\| + K_M \|e_M\| (w_{M_L} \|e_{w_L}\| - \|e_{w_L}\|^2) \\ &\quad + \sum_{i=1}^{L-1} \|e_M\| \|e_{b_i}\| 2H_{M_i} \|\hat{b}_L\| \\ &\quad + K_M \|e_M\| \sum_{i=1}^{L-1} \left(b_{M_i} \|e_{b_i}\| - \|e_{b_i}\|^2 \right) \\ &\quad + \|e_M\| \|e_{b_L}\| + K_M \|e_M\| (b_{M_L} \|e_{b_L}\| - \|e_{b_L}\|^2) \end{aligned} \tag{25}$$

Let $T_{M_i} = -\beta_i B_M^T G_M^{-T} C_M^T C_M$, $R_{M_i} = -\gamma_i B_M^T G_M^{-T} C_M^T C_M$ for $i = 1 \ldots L-1$, $K_{M_{2_i}} = \frac{K_M w_{M_L} + \|T_{M_L}\| + \|P_M\| \sigma_0^M}{2\left(K_M - K_{M_i}^2 (L-1)\right)}$ and $K_{M_{3_i}} = \frac{2K_{M_i} w_{M_L} + K_M w_{M_i}}{2(K_M - 1)}$. Considering the terms which involve e_{w_i} and e_{w_L} in (25) and introducing $2K_{M_i} = \|T_{M_i}\| \prod_{j=1}^{L-1} \sigma_{M_i}$. After addition and subtraction of the terms $K_{M_{2_i}}^2 \|e_M\|$ and $K_{M_{3_i}}^2 \|e_M\|$, we get the following simplified expression:

$$\begin{aligned} &\|e_M\| \left(\frac{1}{L-1} \|P_M\| \sigma' + \left(\frac{K_M}{L-1} - K_{M_i}^2 \right) K_{M_{2i}} \right. \\ &\quad + (K_M - 1)) K_{M_{3i}}^2 - \left(\frac{K_M}{L-1} - K_{M_i}^2 \right) \left(K_{M_{2i}} - \|e_{w_L}\|^2 \right) \\ &\quad \left. - (K_M - 1) \left(K_{M_{3_i}} - \|e_{w_i}\|^2 \right) - \left(K_{M_i} \|e_{w_L}\| - \|e_{w_i}\|^2 \right) \right) \end{aligned} \tag{26}$$

(a) Suppose $\frac{K_M}{L-1} > K_{M_i}^2$, $K_M > 1 \implies K_M > (L-1) K_{M_i}^2$ and $K_M > 1$ for $i = 1 \cdots L-1$.
Let $H_{M_{2i}} = \frac{K_M b_{M_L} + 1 + \|P_M\|}{2\left(K_M - H_{M_i}^2 (L-1)\right)}$ and $H_{M_{3i}} = \frac{2H_{M_i} b_{M_L} + K_M b_{M_i}}{2(K-1)}$
Considering the terms which involve e_{b_i} and e_{b_L} in (25), and assuming $2H_{M_i} = \|R_{M_i}\| \prod_{j=i}^{L-1} \sigma_{m_j}$. After addition and subtraction of the terms $H_{M_{2_i}}^2 \|e_M\|$ and $H_{M_{3_i}}^2 \|e_M\|$, we get the following simplified expression:

$$\begin{aligned} &\|e_M\| \left(-\|e_{b_L}\|^2 \left(\frac{K_M}{L-1} - H_{M_i}^2 \right) + \|e_{b_L}\| \left(\frac{K_M b_{M_L}}{L-1} \right. \right. \\ &\quad \left. + \frac{1}{L-1} + \frac{\|P_M\|}{L-1} \right) + \|e_{b_i}\| \left(K_M b_{M_i} + 2H_{M_i} \left(b_{M_L} \right) \right) \\ &\quad \left. - \left(H_{M_i} \|e_{b_L}\| - \|e_{b_i}\|^2 \right) - \|e_{b_i}\|^2 (K_M - 1) \right) \\ &= \|e_M\| \left(\frac{K_M}{L-1} - H_{M_i}^2 \right) H_{M_{2i}}^2 + (K_M - 1) H_{M_{3i}}^2 \\ &\quad - \left(\frac{K_M}{L-1} - H_{M_i}^2 \right) \left(H_{M_{2i}} - \|e_{b_L}\| \right)^2 - (K_M - 1) \\ &\quad \times \left(H_{M_{3i}} - \|e_{b_i}\| \right)^2 - \left(H_{M_i} \|e_{b_L}\| - \left\| e_{M_{b_i}} \right\| \right)^2 \end{aligned} \tag{27}$$

b) Suppose $\frac{K_M}{L-1} > H_{M_i}^2$ and $K_M > 1 \implies K_M > (L-1) H_{M_i}^2$ and $K_M > 1$ for $i = 1 \cdots L-1$

Presuming (a) and (b) are fulfilled:

$$\begin{aligned} \dot{g} &\leq -\frac{1}{2} \eta_{min} Q_M \|e_M\|^2 + \|e_M\| \|P_M\| \sigma' \\ &\quad + \sum_{i=1}^{L-1} \left(\frac{K_M}{L-1} - K_{M_i}^2 \right) K_{M_{2i}}^2 + \sum_{i=1}^{L-1} (K_M - 1) K_{M_{3i}}^2 \\ &\quad + \sum_{i=1}^{L-1} \left(\frac{K_M}{L-1} - H_{M_i}^2 \right) H_{M_{2i}}^2 - \sum_{i=1}^{L-1} (K_M - 1) H_{M_{3i}}^2 \end{aligned} \tag{28}$$

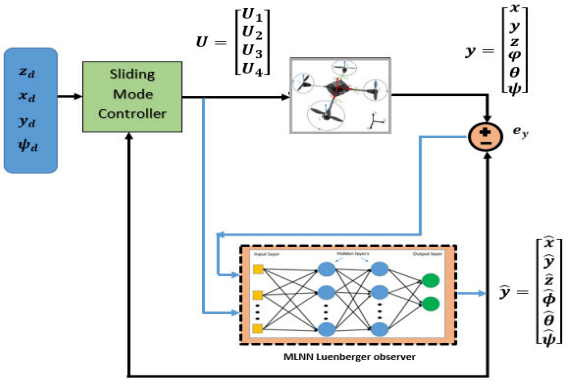

FIGURE 2. Overall controller and MLNN observer design.

To show that $\dot{g}$ is negative definite

$$\|e_M\| > \frac{2\left(\begin{array}{c}\|P_M\|\sigma'+\sum_{i=1}^{L-1}\left(\frac{K_M}{L-1}-K_{M_i}^2\right)K_{M_{2i}}^2+\sum_{i=1}^{L-1}(K_M-1)\\ K_{M_{3i}}^2+\sum_{i=1}^{L-1}\left(\frac{K_M}{L-1}-H_{M_{2i}}^2\right)-\sum_{i=1}^{L-1}(K_M-1)H_{M_{3i}}^2\end{array}\right)}{\eta_{min}(Q_M)} \tag{29}$$

The aforementioned condition must be satisfied for $\|e_M\|$ to ensure that g is negative definite. These equations indicate that the error converges, confirming the stability of the observer.

B. SLIDING MODE CONTROLLER DESIGN

Sliding mode theory is recognized in the literature for its robustness in controller designs specifically for matched disturbances [40], [41], [42]. This study proposes an MLNN observer-based SMC. Therefore, the states estimated by the MLNN observer are provided to the SMC to track the reference altitude and attitude trajectories as shown in Figure 2. The quadrotor model is split into three parts, each with its controller, namely:

1. Altitude (z position) controller, 2. X-Y translational controller, and 3. Attitude (angle) controller.

The SMC calculates four control inputs for controlling, roll, pitch, yaw, and overall thrust. The input to the altitude controller is the desired altitude, while the output is which controls the overall UAV thrust. Similarly, the inputs to the X-Y controller are the desired x and y positions (x_d, y_d), while the outputs are the desired roll and pitch angles (ϕ_d, θ_d). These are fed as input into the attitude controller which is responsible for providing the two control inputs i.e., U_2 and U_3. The SMC design is described in Figure 3.

1) CONTROL LAW SYNTHESIS

The SMC design process consists of two steps, firstly, an appropriate sliding surface design and then, a switching control law design that slides the trajectories to that surface. The chosen sliding surface is defined as [44]:

$$s_k = \dot{e}_k + k_{d_{z_k}} e_k + k_{p_{z_k}} \int_0^t e_k \tag{30}$$

Here $k_{d_{z_k}}, k_{p_{z_k}} > 0$ are selected gains and e_k are error values, which are given as:

$$\begin{cases} e_k = x_{k_d} - \hat{x}_k \\ e_{k+1} = \dot{e}_k \end{cases} \tag{31}$$

where $k = [1, 3, 5, 7, 9, 11]$. $x_{k_d}, \hat{x}_k$ are the k^{th} desired and estimated state respectively and described in detail in subsequent analysis. The SMC switching function is:

$$s_k = \begin{cases} -1 & if\ s_k > 0 \\ 0 & if\ s_k = 0 \\ 1 & if\ s_k < 0 \end{cases} \tag{32}$$

and

$$sign(s_k) = \begin{cases} 1 & if\ s_k > 0 \\ 0 & if\ s_k = 0 \\ -1 & if\ s_k < 0 \end{cases} \tag{33}$$

To eliminate the chattering effect associated with the SMC, the $sign(s_k)$ function is replaced with a saturation function using a boundary layer method which is given in the following equation:

$$sat(s_k) = \begin{cases} sign(s_k) & if\ |s_k| \geq p_k \\ \dfrac{s_k}{p_k} & if\ |s_k| < p_k \end{cases} \tag{34}$$

Here p_k is the boundary layer around s_k [39], [45] used to reduce the chattering problem. In this paper, the modified sliding surfaces with integral terms are as follows [44]:

$$\begin{cases} s_1 = s_{x_1} = \dot{e}_1 + k_{d_{z_1}} e_1 + k_{p_{z_1}} \int_0^t e_1 \\ s_3 = s_{x_3} = \dot{e}_3 + k_{d_{z_3}} e_1 + k_{p_{z_3}} \int_0^t e_3 \\ s_5 = s_{x_5} = \dot{e}_5 + k_{d_{z_5}} e_1 + k_{p_{z_5}} \int_0^t e_5 \\ s_7 = s_{x_7} = \dot{e}_7 + k_{d_{z_7}} e_1 + k_{p_{z_7}} \int_0^t e_7 \\ s_9 = s_{x_9} = \dot{e}_9 + k_{d_{z_9}} e_1 + k_{p_{z_9}} \int_0^t e_9 \\ s_{11} = s_{x_{11}} = \dot{e}_{11} + k_{d_{z_{11}}} e_1 + k_{p_{z_{11}}} \int_0^t e_{11} \end{cases} \tag{35}$$

The sliding mode control laws are as follows [39]:

$$\begin{cases} U_1 = \dfrac{m}{cos\hat{x}_7 cos\hat{x}_9}(g + \ddot{x}_{5_d} + k_{d_{z_5}} \dot{e}_5 \\ \quad + k_{p_{z_5}} e_5 + k_{s_{z_5}} sat(s_5)) \\ U_2 = \dfrac{I_x}{l}(-\hat{x}_{10}\hat{x}_{12}\dfrac{I_y - I_z}{I_x} + \dfrac{I_r}{I_x}\hat{x}_{10}\Omega + \ddot{x}_{7_d} + k_{d_{z_7}} \dot{e}_7 \\ \quad + k_{s_{z_7}} sat(s_7) + k_{p_{z_7}} e_7) \\ U_3 = \dfrac{I_y}{l}(-\hat{x}_8\hat{x}_{12}\dfrac{I_z - I_x}{I_y} + \dfrac{I_r}{I_y}\hat{x}_8\Omega + \ddot{x}_{9_d} + k_{d_{z_9}} \dot{e}_9 \\ \quad + k_{s_{z_9}} sat(s_9) + k_{p_{z_9}} e_9) \\ U_4 = \dfrac{I_z}{l}(-\hat{x}_8\hat{x}_{10}\dfrac{I_x - I_y}{I_z} + \ddot{x}_{11_d} + k_{d_{z_{11}}} \dot{e}_{11} \\ \quad + k_{s_{z_{11}}} sat(s_{11}) + k_{p_{z_{11}}} e_{11}) \end{cases} \tag{36}$$

Here $\dot{x}_{5_d}, \dot{x}_{7_d}, \dot{x}_{9_d}, \dot{x}_{11_d}$ are the derivatives of the desired state trajectories x_5, x_7, x_9, x_{11}, respectively.

IV. NONLINEAR SIMULATION RESULTS

A. TRAINING DATA

The training data used for MLNN observer is generated using the nonlinear quadrotor UAV model, as discussed in the previous section. There are a total of 10 inputs to the neural network: four control inputs, U_1, U_2, U_3 and U_4, and six state errors $e_1, e_3, e_5, e_7, e_9, e_{11}$, while the outputs are the estimated states shown in Figure 2. The neural network is trained using input-output data to estimate states that closely match the actual ones. The neural network comprises four hidden layers, each with 10, 15, 20, and 15 neurons, respectively, all having a sigmoid activation function. The initial weights and bias terms of the network are initialized with small random numbers, and these weights are trained and updated using the back-propagation algorithm. After the training phase, the next step is to use the trained neural network model, along with the weights and biases obtained during training, in run-time simulations to estimate the states online and assess the effectiveness of the neural network observer.

In this section, a comprehensive comparison of the proposed MLNN-based Luenberger observer is performed with the SHLNN [36] and SMO [14] under parameter variations, wind disturbances, and sensor noise.

Unit step reference commands are applied to the x and y positions. The desired z position is a ramp input from 0 to 50 seconds with a maximum height of 15 meters. The desired yaw angle is kept at zero. The desired trajectory of the quadrotor is such that it takes off from its starting position of (0,0,0) meters and after passing through the waypoint of (15,1,1) meters, it returns to the final position of (5,0,0) meters. The initial conditions for the x, y, and z states are random. For simulating real flight conditions, wind gust using the Dryden wind gust model [47] is summed up in the non-linear plant equations. The disturbance effects are added for state estimation in the simulation results. A noise block having variance = 0.01, seed value = 1, and sample time = 0.1 is used. These values are added in the six available states.

To reflect the efficacy of the proposed MLNN observer, the proposed scheme is tested under three cases of parameter variations. These three cases of parameter variations are discussed in Table 2 and the controller and observer gains are given in Table 3.

B. ACTUATOR DYNAMICS

To incorporate the effects of friction caused by the actuator, we introduced first-order actuator dynamics into the simulation, along with the time delay inspired by the work [48], [49]. The equation for the first-order actuator taken from [49] is as follows:

$$Act = \frac{e^{-Ts}}{\beta s + 1}$$

where β is the friction coefficient and T= 0.25 sec.

C. RESULTS FOR NOMINAL PARAMETERS CASE WITH MEASUREMENT NOISE AND DISTURBANCE EFFECTS (CASE A)

Figure 4 displays the state estimation results of the proposed MLNN-based Luenberger observer as compared to SMO and SHLNN observer for nominal Case A. The states to be estimated are x, y, z, ϕ(roll), θ(pitch), and ψ(yaw). The SMO is sensitive to noise, showing quite oscillatory behavior as compared to SHLNN and MLNN observers. Disturbances and noise typically introduce non-linearities into the data. In handling these non-linearities, multilayer neural networks (MLNNs) exhibit a clear advantage over single-layer networks, which are constrained to linear mappings. Figure 4 highlights the improved performance of the proposed MLNN observer in the presence of disturbances and noise. In Figure 4(a), the SHLNN estimated x-position trajectory deviates from the reference trajectory from 0 to 30 seconds. Similarly, in Figure 4(b), the SHLNN estimated y-trajectory deviates from the reference trajectory between 25 to 40 seconds. The SHLNN results in Figures 4(d) and 4(f) also display continuous deviations from the reference trajectories. The estimation states of SMO show the highest oscillations. While the MLNN observer effectively rejects measurement noise and estimates the states close to the reference states with minimal error as compared to SMO, and SHLNN observer.

D. STATE ESTIMATION RESULTS WITH NOISE AND DISTURBANCE DURING PARAMETER VARIATIONS (CASE B AND C)

The parameters of UAVs such as mass (m), the moment of inertias along the x, y and z-axis (Ix, Ix, Iz), drag forces (b), and coefficient of thrust(d) might change due to aerodynamic disturbances and uncertainties during flight. This subsection discusses the effectiveness of the proposed MLNN observer when the parameters vary from the nominal Case A, specifically in Cases B and C, in the presence of noise and disturbance effects. Figures 5 and 6 illustrate the state estimation comparison between SMO, SHLNN, and MLNN observers.

In Figure 5, the state estimation comparison under Case B reveals that SMO trajectories exhibit considerable noise and substantial errors between the actual and SMO trajectories. The results obtained from the SHLNN observer are less noisy compared to SMO; however, they diverge from reference trajectories at certain time points, as observed in Figure 5(b, d, and e). In contrast, the proposed MLNN observer successfully tracks the actual trajectories with less noisy results compared to the other two observers.

In Figure 6, a state estimation comparison under Case C parameter values is presented. SMO's estimated trajectories deviate further from the reference and actual trajectories compared to Cases A and B. This behavior is attributed to SMO's limited adaptability to changing parameters. The state estimation results of SHLNN observer exhibit less noisy

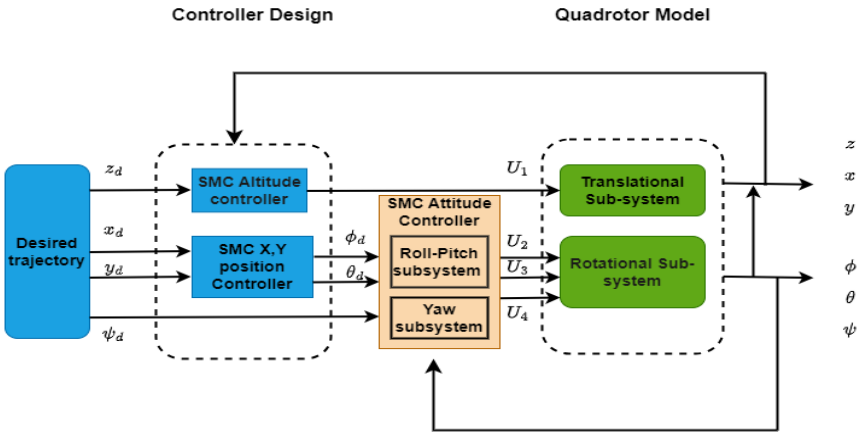

FIGURE 3. The SMC controller design.

TABLE 2. Parametric variations.

Parameters	Case A	Case B	Case C
mass m (kg)	0.65	1.7	2.3
Moment of Inertia along x I_{p_x} (kgm^2)	$7.5\text{x}10^{-3}$	$9\text{x}10^{-3}$	$11\text{x}10^{-3}$
Moment of Inertia along yI_{p_y} (kgm^2)	$7.5\text{x}10^{-3}$	$9\text{x}10^{-3}$	$11\text{x}10^{-3}$
Moment of Inertia along zI_{p_z} (kgm^2)	$1.3\text{x}10^{-2}$	$2\text{x}10^{-2}$	$3\text{x}10^{-2}$
Thrust coefficient b (Ns^2)	$3.13\text{x}10^{-5}$	$3.5\text{x}10^{-5}$	$4\text{x}10^{-5}$
Drag coefficient d (Nms^2)	$7.5\text{x}10^{-7}$	$8\text{x}10^{-7}$	$8.5\text{x}10^{-7}$

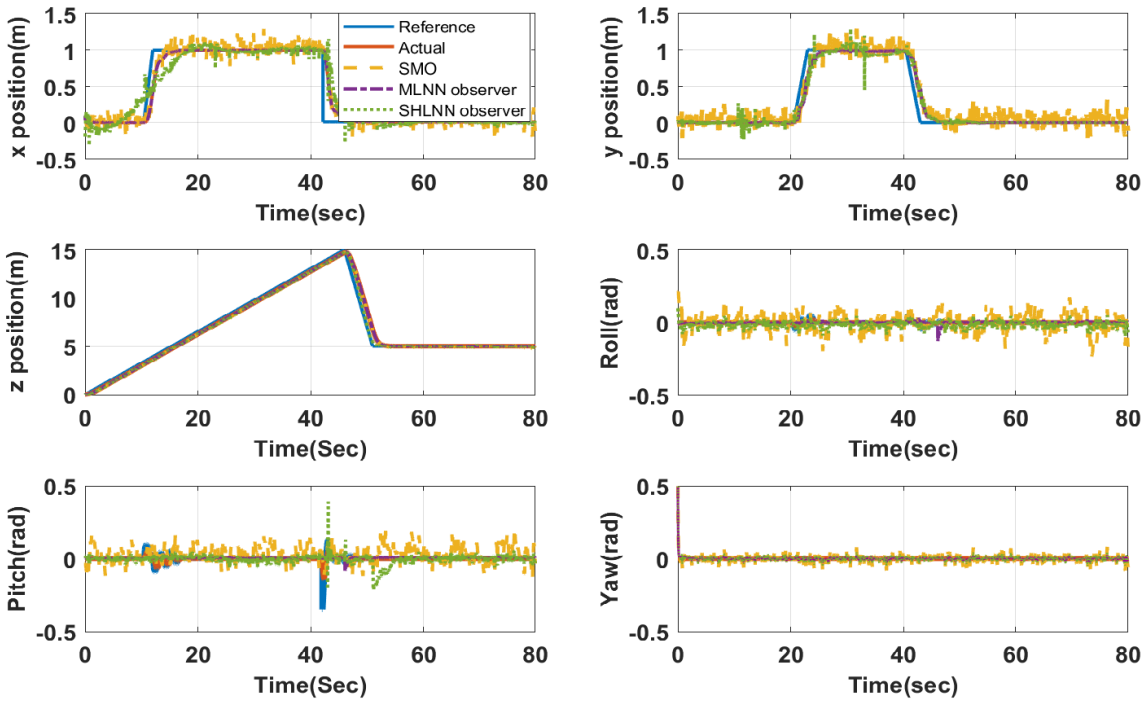

FIGURE 4. Case A: Estimated positions and angular states of SMO, SHLNN, and MLNN observers.

and good estimation as compared to SMO. Figure 6(a, c, d, f) shows continuous deviations, while in Figure 6(b), SHLNN deviates from the reference y-position between 10 to 60 seconds.

The estimated SHLNN pitch trajectory is shown in Figure 6(e), with the deviation from the reference pitch occurring between 20 to 40 seconds. However, the MLNN observer outperforms both SMO and SHLNN observers due

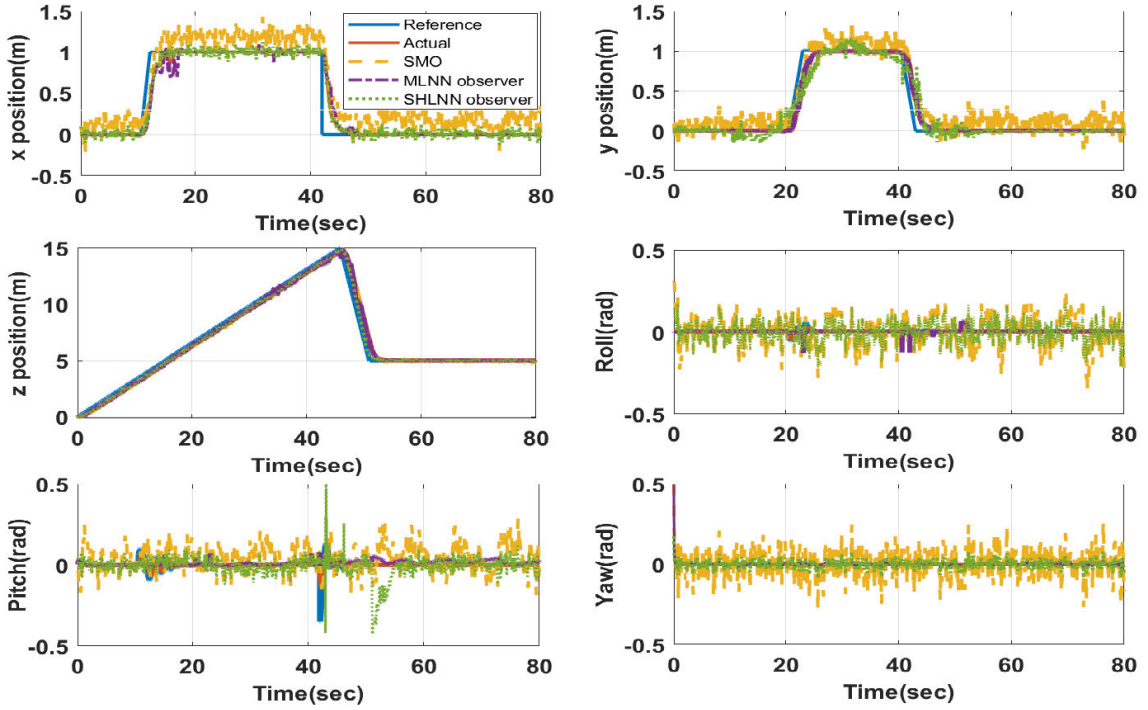

FIGURE 5. Case B: Estimated positions and angular states of SMO, SHLNN, and MLNN observers.

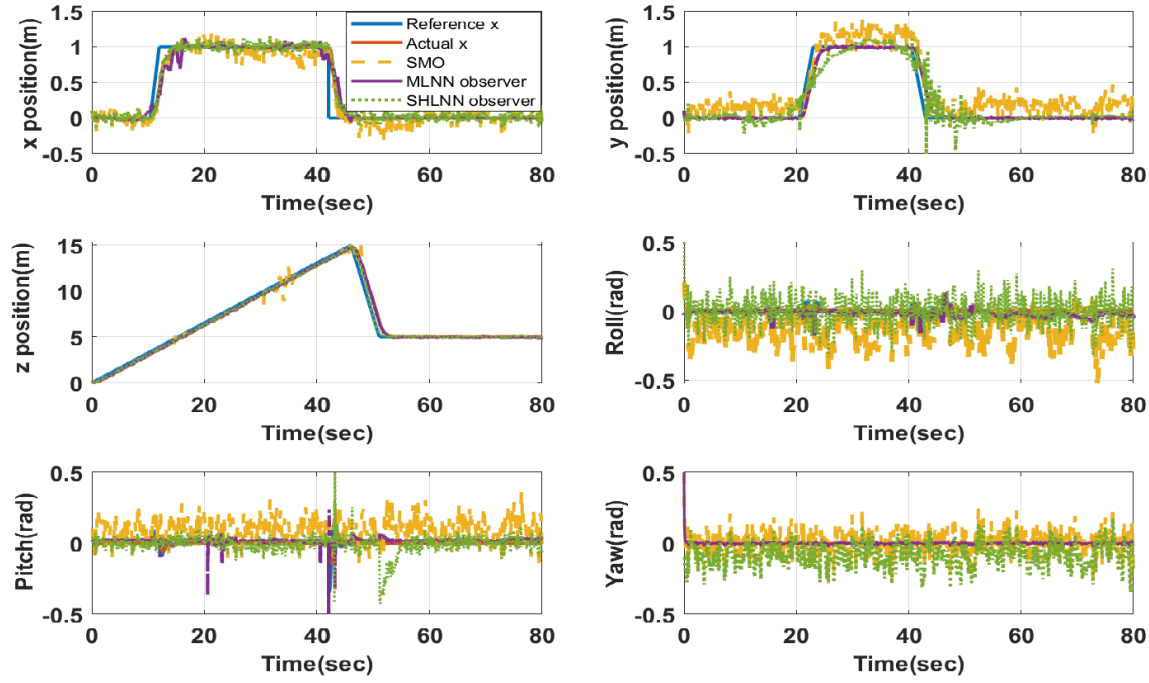

FIGURE 6. Case C: Estimated positions and angular states of SMO, SHLNN, and MLNN observers.

to its adaptive nature by estimating trajectories closer to the reference trajectories.

In summary, the state estimation results for all three cases of parameter variations, as shown in Figures 4, 5, and 6, demonstrate the superior performance of MLNN observers compared to SMO and SHLNN observers in terms of handling parameter variations, noise, and disturbances. For a more detailed understanding, the numerical values of these errors, in terms of Mean Square Error (MSE), are presented in Table 4.

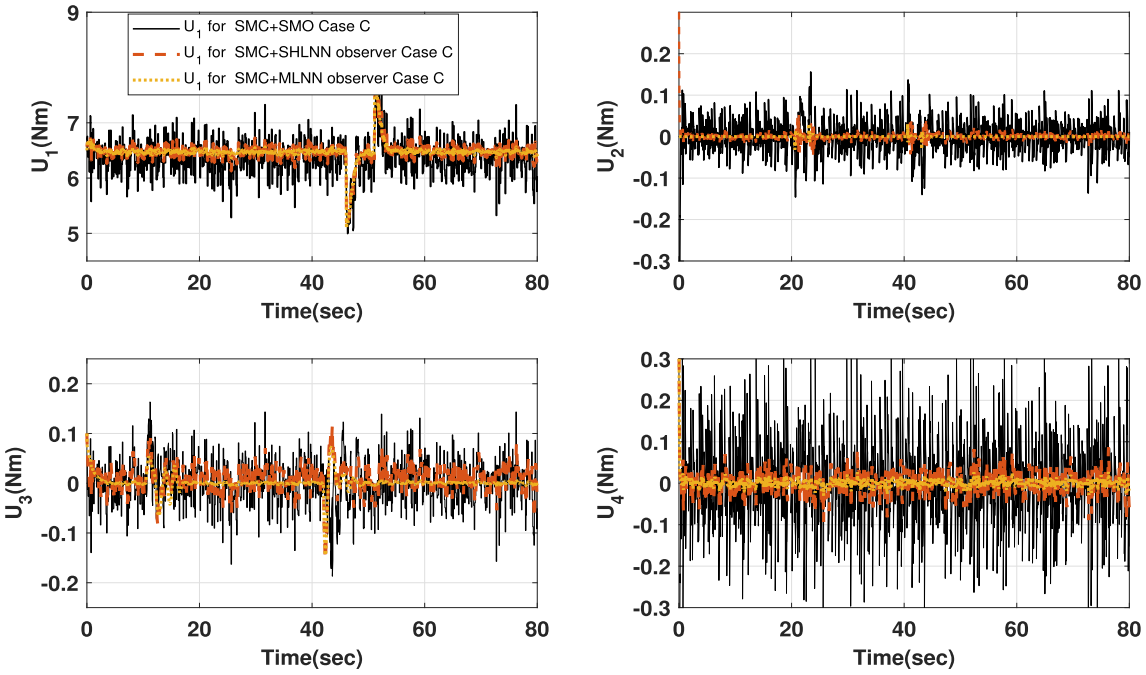

FIGURE 7. Control input torques.

TABLE 3. Controller and observer gain values.

Gains	Values	Gains	Values
$k_{p_{z_1}}$	0.01	$k_{p_{z_9}}$	0.025
$k_{d_{z_1}}$	1	$k_{d_{z_9}}$	3.5
$k_{s_{z_1}}$	4	$k_{s_{z_9}}$	6
$k_{p_{z_3}}$	0.002	$k_{p_{z_{11}}}$	0.0002
$k_{d_{z_3}}$	1	$k_{d_{z_{11}}}$	2.5
$k_{s_{z_3}}$	3.75	$k_{s_{z_{11}}}$	5
$k_{p_{z_5}}$	5.25	δ	248
$k_{d_{z_5}}$	3.75	K	0.008
$k_{s_{z_5}}$	5.5	η	300
$k_{p_{z_7}}$	0.025	$k_{d_{z_7}}, k_{s_{z_7}}$	3.5, 6

E. CONTROL INPUT RESULTS UNDER CASE C PARAMETER VARIATION

To demonstrate the effectiveness of the control strategy, control input results under worst-case parameter values C are presented in Figure 7. The figure shows the control input comparison when SMC receives estimated states information from three observers namely, Multi-layer NN (MLNN), Single Hidden Layer NN (SHLNN) and Sliding Mode Observer (SMO).

Figure 7(a) presents the comparison results for the control input U1 for the three observers. U1 for the Sliding Mode Control with Multi-Layer Neural Network (SMC + MLNN) observer demonstrates the least noise and divergence, gradually rising after 45 seconds to follow the altitude's trajectory. Meanwhile, U1 for both SMO and SHLNN observers with SMC also experiences a rise after 45 seconds, but with noticeable noise and divergence.

Similarly, Figure 7(b) illustrates the comparison of U2, associated with the roll angle, for the three observers. In all three cases, U2 increases at 20 and 40 seconds, respectively. However, U2 for SHLNN and SMO exhibits more noise compared to the MLNN observer, with the latter being the most noisy. Figures 7(c) and (d) depict the comparison results for U3 and U4, associated with pitch and yaw angle respectively. U3 experiences a rise at 10 and 40 seconds. The comparison results indicate that MLNN + SMC yields the least noisy results, as compared to SHLNN and SMO.

The comprehensive analysis of control inputs in Figures 7 reveals that the MLNN observer consistently produces less noisy results than both the SMO and SHLNN observers, as desired.

In Table 4, a comparison of Mean Square Error (MSE) is presented between SMO, SHLNN, and MLNN observers. The MSE values for are measured in square meters (m^2), while for, and, the units are square radians (rad^2). SMO exhibits the highest MSE values for state estimation in all three cases. In contrast, the SHLNN observer shows lower MSE values than SMO. The MLNN observer demonstrates the lowest MSE values, making it *e* preferred choice for state estimation in this particular application.

The formula used for MSE for continuous-time signals is:

$$MSE = \frac{1}{t_2 - t_1} \int_{t_1}^{t_2} (e(t))^2 dt$$

where $e(t)$ is the error between ith actual and estimated state. is the length of the signal. We used the mean() command in Matlab, giving a square of error as input for finding the MSE values.

TABLE 4. Comparison between SMO, MLNN, and SHLNN observer techniques in terms of MSE.

Estimated states	Mean square error								
	Sliding Mode Observer			MLNN observer			SHLNN observer		
	Case A	Case B	Case C	Case A	Case B	Case C	Case A	Case B	Case C
$\hat{x}$	$6.25\text{x}10^{-2}$	$7.05\text{x}10^{-1}$	$9.35\text{x}10^{-1}$	$1.6\text{x}10^{-3}$	$5.2\text{x}10^{-3}$	$7.6\text{x}10^{-2}$	$2.2\text{x}10^{-2}$	$3.8\text{x}10^{-2}$	$5.8\text{x}10^{-2}$
$\hat{y}$	$3.5\text{x}10^{-2}$	$4.56\text{x}10^{-1}$	$4.89\text{x}10^{-1}$	$2.01\text{x}10^{-3}$	$3.8\text{x}10^{-3}$	$2.6\text{x}10^{-2}$	$1.4\text{x}10^{-2}$	$2.3\text{x}10^{-2}$	$3.5\text{x}10^{-2}$
$\hat{z}$	$1.01\text{x}10^{-3}$	$2.03\text{x}10^{-3}$	$2.6\text{x}10^{-3}$	$3.08\text{x}10^{-4}$	$6.2\text{x}10^{-4}$	$9.08\text{x}10^{-4}$	$8.1\text{x}10^{-4}$	$9.2\text{x}10^{-4}$	$1.3\text{x}10^{-3}$
$\hat{\phi}$	$3.8\text{x}10^{-2}$	$3.1\text{x}10^{-1}$	$2.55\text{x}10^{-1}$	$1.75\text{x}10^{-3}$	$3.1\text{x}10^{-3}$	$3.8\text{x}10^{-3}$	$1.6\text{x}10^{-2}$	$5.2\text{x}10^{-2}$	$7.6\text{x}10^{-2}$
$\hat{\theta}$	$4.01\text{x}10^{-2}$	$2.6\text{x}10^{-1}$	$2.02\text{x}10^{-1}$	$1.3\text{x}10^{-3}$	$2.5\text{x}10^{-3}$	$4.8\text{x}10^{-3}$	$2.6\text{x}10^{-3}$	$5.2\text{x}10^{-3}$	$7.7\text{x}10^{-2}$
$\hat{\psi}$	$3.2\text{x}10^{-2}$	$2.1\text{x}10^{-1}$	$1.25\text{x}10^{-1}$	$3.6\text{x}10^{-4}$	$4.6\text{x}10^{-4}$	$7.3\text{x}10^{-4}$	$3.5\text{x}10^{-3}$	$5.7\text{x}10^{-3}$	$6.6\text{x}10^{-2}$

V. CONCLUSION

The paper proposes an adaptive multi-layer neural network-based Luenberger observer in which the weights are updated using a modified back-propagation algorithm and compares it with the SMO and SHLNN observer using a dynamical non-linear model of a quadrotor UAV. We ensured the Lyapunov stability of the proposed observer using a modified back-propagation weight update rule, which, to the best of the author's knowledge, is not present in the literature. To replicate the signal transmission delay and actuator friction effects in the model, we added a first-order delay in the actuator dynamics. The results of the proposed observer technique are compared with those of the SMO and SHLNN observer in the presence of wind disturbance, noise, and parameter variations in terms of Mean Square Error (MSE) values. The proposed observer produces less noisy estimation results in the presence of all of these parameters as compared to the other two observers.

FUTURE DIRECTIONS

Future work aims to implement the proposed observer-based control scheme on a real quadrotor. Additionally, we intend to design a Fault Detection and Isolation scheme (FDI) that utilizes state estimation results from the proposed observer. Updated information from the FDI could then be incorporated into a Fault-Tolerant Control framework, which will be tested on a real quadrotor to improve system control during abnormal conditions.

In recent years output feedback control techniques has gained importance due to shortcomings encountered when full-state measurements are unavailable. The paper in [50] presents an adaptive output feedback neural network-based control method for underactuated and unactuated state constraints without the need for exact model knowledge. The study [51] suggests a control approach that utilizes neuroadaptive methods to address challenges posed by simultaneous output and velocity constraints on both actuated and unactuated states. We intend to test our proposed algorithm under such state-constraint conditions.

REFERENCES

[1] G. Ononiwu, O. Onojo, O. Ozioko, and O. Nosiri, "Quadcopter design for payload delivery," *J. Comput. Commun.*, vol. 4, no. 10, pp. 1–12, 2016.

[2] V. Duggal, M. Sukhwani, K. Bipin, G. S. Reddy, and K. M. Krishna, "Plantation monitoring and yield estimation using autonomous quadcopter for precision agriculture," in *Proc. IEEE Int. Conf. Robot. Autom. (ICRA)*, May 2016, pp. 5121–5127.

[3] S. Bouabdallah, *Design and Control of Quadrotors With Application to Autonomous Flying*. Vaud, Switzerland: EPFL, 2007.

[4] X. Lyu, J. Zhou, H. Gu, Z. Li, S. Shen, and F. Zhang, "Disturbance observer based hovering control of quadrotor tail-sitter VTOL UAVs using H_∞ synthesis," *IEEE Robot. Automat. Lett.*, vol. 3, no. 4, pp. 2910–2917, Jun. 2018.

[5] J. Zhao, S. Tong, and Y. Li, "Observer-based fuzzy adaptive control for MIMO nonlinear systems with non-constant control gain and input delay," *IET Control Theory Appl.*, vol. 15, no. 11, pp. 1488–1505, Jul. 2021.

[6] S. Tong, Y. Li, and P. Shi, "Observer-based adaptive fuzzy backstepping output feedback control of uncertain MIMO pure-feedback nonlinear systems," *IEEE Trans. Fuzzy Syst.*, vol. 20, no. 4, pp. 771–785, Aug. 2012.

[7] J.-J. Xiong and E.-H. Zheng, "Optimal Kalman filter for state estimation of a quadrotor UAV," *Optik*, vol. 126, no. 21, pp. 2862–2868, Nov. 2015.

[8] T. Zhang and Y. Liao, "Attitude measure system based on extended Kalman filter for multi-rotors," *Comput. Electron. Agricult.*, vol. 134, pp. 19–26, Mar. 2017.

[9] H. B. Khamseh, S. Ghorbani, and F. Janabi-Sharifi, "Unscented Kalman filter state estimation for manipulating unmanned aerial vehicles," *Aerosp. Sci. Technol.*, vol. 92, pp. 446–463, Sep. 2019.

[10] W. Cai, J. She, M. Wu, and Y. Ohyama, "Disturbance suppression for quadrotor UAV using sliding-mode-observer-based equivalent-input-disturbance approach," *ISA Trans.*, vol. 92, pp. 286–297, Sep. 2019.

[11] Z. Zhao, D. Cao, J. Yang, and H. Wang, "High-order sliding mode observer-based trajectory tracking control for a quadrotor UAV with uncertain dynamics," *Nonlinear Dyn.*, vol. 102, no. 4, pp. 2583–2596, Dec. 2020.

[12] W. Chen and M. Saif, "Novel sliding mode observers for a class of uncertain systems," in *Proc. Amer. Control Conf.*, Jun. 2006, p. 6.

[13] Y.-S. Kung, N. V. Quynh, C.-C. Huang, and L.-C. Huang, "Design and simulation of adaptive speed control for SMO-based sensorless PMSM drive," in *Proc. 4th Int. Conf. Intell. Adv. Syst. (ICIAS)*, vol. 1, Jun. 2012, pp. 439–444.

[14] L. Chen, C. Edwards, H. Alwi, M. Sato, S. Nateghi, and Y. Shtessel, "Sliding mode observers for robust fault estimation in linear parameter varying systems," *Int. J. Robust Nonlinear Control*, vol. 33, no. 15, pp. 9084–9108, Oct. 2023.

[15] C. Edwards, S. K. Spurgeon, and R. J. Patton, "Sliding mode observers for fault detection and isolation," *Automatica*, vol. 36, no. 4, pp. 541–553, Apr. 2000.

[16] J. Du, X. Hu, H. Liu, and C. L. P. Chen, "Adaptive robust output feedback control for a marine dynamic positioning system based on a high-gain observer," *IEEE Trans. Neural Netw. Learn. Syst.*, vol. 26, no. 11, pp. 2775–2786, Nov. 2015.

[17] H. Xu and J. Wang, "Distributed observer-based control law with better dynamic performance based on distributed high-gain observer," *Int. J. Syst. Sci.*, vol. 51, no. 4, pp. 631–642, Mar. 2020.

[18] S. Nicosia and A. Tornambè, "High-gain observers in the state and parameter estimation of robots having elastic joints," *Syst. Control Lett.*, vol. 13, no. 4, pp. 331–337, Nov. 1989.

[19] J. Muliadi and B. Kusumoputro, "Neural network control system of UAV altitude dynamics and its comparison with the PID control system," *J. Adv. Transp.*, vol. 2018, pp. 1–18, Jan. 2018.

[20] W. Gu, K. P. Valavanis, M. J. Rutherford, and A. Rizzo, "UAV model-based flight control with artificial neural networks: A survey," *J. Intell. Robotic Syst.*, vol. 100, nos. 3–4, pp. 1469–1491, Dec. 2020.
[21] Y.-J. Liu, S. Tong, and C. L. P. Chen, "Adaptive fuzzy control via observer design for uncertain nonlinear systems with unmodeled dynamics," *IEEE Trans. Fuzzy Syst.*, vol. 21, no. 2, pp. 275–288, Apr. 2013.
[22] Y. Ma and Y. Cai, "A fuzzy model predictive control based upon adaptive neural network disturbance observer for a constrained hypersonic vehicle," *IEEE Access*, vol. 6, pp. 5927–5938, 2018.
[23] D. Wang, Q. Zong, B. Tian, S. Shao, X. Zhang, and X. Zhao, "Neural network disturbance observer-based distributed finite-time formation tracking control for multiple unmanned helicopters," *ISA Trans.*, vol. 73, pp. 208–226, Feb. 2018.
[24] T. Matassini, H.-S. Shin, A. Tsourdos, and M. Innocenti, "Adaptive control with neural networks-based disturbance observer for a spherical UAV," *IFAC-PapersOnLine*, vol. 49, no. 17, pp. 308–313, 2016.
[25] Z. Zhou, X. Li, W. Tuo, and F. Wang, "Design of active disturbance rejection control with noise observer for an optical reference unit," *Control Eng. Pract.*, vol. 132, Mar. 2023, Art. no. 105427.
[26] M. N. Ibarra-Bonilla, P. J. Escamilla-Ambrosio, and J. M. Ramirez-Cortes, "Attitude estimation using a neuro-fuzzy tuning based adaptive Kalman filter," *J. Intell. Fuzzy Syst.*, vol. 29, no. 2, pp. 479–488, Oct. 2015.
[27] P. Aboutalebi, A. Abbaspour, P. Forouzannezhad, and A. Sargolzaei, "A novel sensor fault detection in an unmanned quadrotor based on adaptive neural observer," *J. Intell. Robotic Syst.*, vol. 90, nos. 3–4, pp. 473–484, Jun. 2018.
[28] A. Abbaspour, P. Aboutalebi, K. K. Yen, and A. Sargolzaei, "Neural adaptive observer-based sensor and actuator fault detection in nonlinear systems: Application in UAV," *ISA Trans.*, vol. 67, pp. 317–329, Mar. 2017.
[29] S. Stebler, M. Campobasso, K. Kidambi, W. MacKunis, and M. Reyhanoglu, "Dynamic neural network-based sliding mode estimation of quadrotor systems," in *Proc. Amer. Control Conf. (ACC)*, May 2017, pp. 2600–2605.
[30] M. A. K. Jaradat and M. F. Abdel-Hafez, "Non-linear autoregressive delay-dependent INS/GPS navigation system using neural networks," *IEEE Sensors J.*, vol. 17, no. 4, pp. 1105–1115, Feb. 2017.
[31] H. Boudjedir, O. Bouhali, and N. Rizoug, "Adaptive neural network control based on neural observer for quadrotor unmanned aerial vehicle," *Adv. Robot.*, vol. 28, no. 17, pp. 1151–1164, Sep. 2014.
[32] B. Zhao, S. Xu, J. Guo, R. Jiang, and J. Zhou, "Integrated strapdown missile guidance and control based on neural network disturbance observer," *Aerosp. Sci. Technol.*, vol. 84, pp. 170–181, Jan. 2019.
[33] A. Lakhal, A. Tlili, and N. B. Braiek, "Neural network observer for nonlinear systems application to induction motors," *Int. J. Control Automat.*, vol. 3, no. 1, pp. 1–16, 2010.
[34] M. Ullah, C. Zhao, H. Maqsood, M. Humayun, and M. U. Hassan, "Exponential sliding mode control based on a neural network and finite-time disturbance observer for an autonomous aerial vehicle exposed to environmental disturbances and parametric uncertainties," *J. Control, Autom. Electr. Syst.*, vol. 33, no. 6, pp. 1659–1670, Dec. 2022.
[35] M. K. Al-Sharman, Y. Zweiri, M. A. K. Jaradat, R. Al-Husari, D. Gan, and L. D. Seneviratne, "Deep-learning-based neural network training for state estimation enhancement: Application to attitude estimation," *IEEE Trans. Instrum. Meas.*, vol. 69, no. 1, pp. 24–34, Jan. 2020.
[36] J. Yuning, M. Ahmad, Q. Bo, G. Farid, and S. Tahir, "An adaptive neural network state estimator for quadrotor unmanned air vehicle," *Int. J. Adv. Comput. Sci. Appl.*, vol. 10, no. 2, pp. 1–6, 2019.
[37] Y. Gao, G. Zhu, and T. Zhao, "Based on backpropagation neural network and adaptive linear active disturbance rejection control for attitude of a quadrotor carrying a load," *Appl. Sci.*, vol. 12, no. 24, p. 12698, Dec. 2022.
[38] S. Langer, "Approximating smooth functions by deep neural networks with sigmoid activation function," *J. Multivariate Anal.*, vol. 182, Mar. 2021, Art. no. 104696.
[39] V. G. Adir, A. M. Stoica, and J. F. Whidborne, "Sliding mode control of a 4Y octorotor," *UPB Sci. Bull., Ser. D*, vol. 74, no. 4, pp. 37–51, 2012.
[40] M. Labbadi and M. Cherkaoui, "Robust adaptive nonsingular fast terminal sliding-mode tracking control for an uncertain quadrotor UAV subjected to disturbances," *ISA Trans.*, vol. 99, pp. 290–304, Apr. 2020.
[41] S. Ullah, A. Mehmood, Q. Khan, S. Rehman, and J. Iqbal, "Robust integral sliding mode control design for stability enhancement of under-actuated quadcopter," *Int. J. Control, Autom. Syst.*, vol. 18, no. 7, pp. 1671–1678, Jul. 2020.
[42] K. Wang, C. Hua, J. Chen, and M. Cai, "Dual-loop integral sliding mode control for robust trajectory tracking of a quadrotor," *Int. J. Syst. Sci.*, vol. 51, no. 2, pp. 203–216, Jan. 2020.
[43] A. Victor G. and S. Adrian M. STOICA, "Integral LQR control of a star-shaped octorotor," *INCAS Bull.*, vol. 4, no. 2, pp. 3–18, Jun. 2012.
[44] M. T. Hamayun, S. Ijaz, and A. H. Bajodah, "Output integral sliding mode fault tolerant control scheme for LPV plants by incorporating control allocation," *IET Control Theory Appl.*, vol. 11, no. 12, pp. 1959–1967, Aug. 2017.
[45] N. B. Cheng, L. W. Guan, L. P. Wang, and J. Han, "Chattering reduction of sliding mode control by adopting nonlinear saturation function," *Adv. Mater. Res.*, vols. 143–144, pp. 53–61, Oct. 2010.
[46] K. S. Narendra and A. M. Annaswamy, *Stable Adaptive Systems*. Chelmsford, MA, USA: Courier Corporation, 2012.
[47] F. M. Hoblit, *Gust Loads on Aircraft: Concepts and Applications*. Reston, VA, USA: AIAA, 1988.
[48] S. K. Armah, S. Yi, and W. Choi, "Design of feedback control for quadrotors considering signal transmission delays," *Int. J. Control, Autom. Syst.*, vol. 14, no. 6, pp. 1395–1403, Dec. 2016.
[49] Y. Qi, Y. Zhu, J. Wang, J. Shan, and H. H. T. Liu, "MUDE-based control of quadrotor for accurate attitude tracking," *Control Eng. Pract.*, vol. 108, Mar. 2021, Art. no. 104721.
[50] T. Yang, N. Sun, and Y. Fang, "Neuroadaptive control for complicated underactuated systems with simultaneous output and velocity constraints exerted on both actuated and unactuated states," *IEEE Trans. Neural Netw. Learn. Syst.*, vol. 34, no. 8, pp. 4488–4498, Oct. 2021.
[51] T. Yang, H. Chen, N. Sun, and Y. Fang, "Adaptive neural network output feedback control of uncertain underactuated systems with actuated and unactuated state constraints," *IEEE Trans. Syst. Man, Cybern. Syst.*, vol. 52, no. 11, pp. 7027–7043, Nov. 2022.

ZAINAB AKHTAR received the M.S. degree in electrical engineering from the Department of Electrical and Computer Engineering, COMSATS University, Lahore, Pakistan, in 2018. She is currently pursuing the Ph.D. degree with the Department of Mechatronics Engineering, University of Engineering and Technology, Pakistan. She was with the Human Centered Robotics Laboratory (HCRL) funded by the Ministry of Science and Technology, Pakistan, from 2018 to 2020. Her research interests include machine learning, intelligent systems, fault-tolerant control of aircraft systems, sliding mode control, and UAV systems.

SYED ABBAS ZILQURNAIN NAQVI received the Ph.D. degree in computer science from Purdue University, USA, in 2016. He is currently an Associate Professor with the Department of Mechatronics, University of Engineering and Technology, Pakistan. His research interests include statistical machine learning, quantum computing, and Bayesian learning.

MIRZA TARIQ HAMAYUN received the Ph.D. degree from the University of Leicester, U.K., in 2013. He is currently an Associate Professor with the Department of Electrical and Computer Engineering, COMSATS University Islamabad, Lahore Campus, Islamabad, Pakistan. He is the author of over 32 refereed articles, including one monograph for Springer-Verlag entitled *Fault Tolerant Control Schemes Using Integral Sliding Modes*. His current research interests include LPV control and integral sliding mode fault tolerant control schemes.

MUHAMMAD AHSAN received the Ph.D. degree from Duke University, USA, in 2015. He is currently an Associate Professor with the Department of Mechatronics Engineering, University of Engineering and Technology, Pakistan. His research interests include fault-tolerant quantum computation, quantum computer architecture design, and analysis of algorithms.

AHSAN NADEEM (Member, IEEE) received the B.Sc. degree in electrical engineering from the University of Engineering and Technology, Lahore, Pakistan, in 2015, the M.S. degree in electrical engineering from COMSATS University, Pakistan, in 2017, and the Ph.D. degree from the GIK Institute, Pakistan, in 2022. From 2016 to 2017, he was the Assistant Manager of Pakistan Telecommunications Company Ltd. (PTCL). From 2018 to 2022, he was a Laboratory Engineer with the GIK Institute. He is currently with the Energy Department, Aalborg University, Denmark. He has published several papers in renowned transactions, journals, and conferences, including IEEE, IET, Elsevier, Springer, and Sage. His research interests include maximum power point tracking (MPPT) and fault detection algorithms for photovoltaic (PV) systems, smart charging of batteries, microgrids, optimization algorithms, and sliding mode control applications in power converters.

S. M. MUYEEN (Fellow, IEEE) received the B.Sc. degree in electrical and electronic engineering from Rajshahi University of Engineering and Technology (RUET, formerly known as Rajshahi Institute of Technology), Bangladesh, in 2000, and the M.Eng. and Ph.D. degrees in electrical and electronic engineering from Kitami Institute of Technology, Japan, in 2005 and 2008, respectively. He is currently a Full Professor with the Department of Electrical Engineering, Qatar University. He has published more than 250 papers in different journals and international conferences. He has also published seven books as the author or an editor. His research interests include power system stability, control systems, electrical machine, FACTS, energy storage systems (ESSs), renewable energy, and HVDC systems. He is a fellow of Engineers Australia. He is serving as an Editor/Associate Editor for many prestigious journals, such as IEEE, IET, and other publishers, including IEEE TRANSACTIONS ON ENERGY CONVERSION, IEEE POWER ENGINEERING LETTERS, *IET Renewable Power Generation*, and *IET Generation, Transmission and Distribution*. He has been a keynote speaker and an invited speaker at many international conferences, workshops, and universities.

ARMAN OSHNOEI (Senior Member, IEEE) received the M.S. degree in electrical engineering from the University of Tabriz, Tabriz, Iran, in 2017, and the Ph.D. degree in electrical engineering from Shahid Beheshti University, Tehran, Iran, in 2021. From November 2020 to May 2021, he was a Visiting Ph.D. Scholar with the Department of Energy, Aalborg University, Aalborg, Denmark. From August 2021 to March 2022, he was a Research Assistant with Aalborg University. From May 2022 to October 2023, he was a Postdoctoral Research Fellow with Aalborg University, where he is currently an Assistant Professor of electrical power engineering. His current research interests include the control and stability of power electronic-based power systems, energy storage systems, and intelligent control. He has been selected and awarded by the National Elite Foundation of Iran, in 2019. He was a recipient of the Outstanding Researcher Award from Shahid Beheshti University, in 2022.

Open Access funding provided by 'Qatar National Library' within the CRUI CARE Agreement